ZnO Film UV Photodetector with Enhanced Performance: Heterojunction with $CdMoO_4$ Microplates and the Hot Electron Injection Effect of Au Nanoparticles

*Weixin Ouyang, Feng Teng, Mingming Jiang, and Xiaosheng Fang**

***A** novel $CdMoO_4$–ZnO composite film is prepared by spin-coating $CdMoO_4$ microplates on ZnO film and is constructed as a heterojunction photodetector (PD). With an optimized loading amount of $CdMoO_4$ microplates, this composite film PD achieves a ≈18-fold higher responsivity than pure ZnO film PD at 5 V bias under 350 nm (0.15 mW cm^{-2}) UV light illumination, and its decay time shortens to half of the original value. Furthermore, Au nanoparticles are then deposited to modify the $CdMoO_4$–ZnO composite film, and the as-constructed photodetector with an optimized deposition time of Au nanoparticles yields an approximately two-fold higher photocurrent under the same condition, and the decay time reduces by half. The introduced $CdMoO_4$ microplates form type-II heterojunctions with ZnO film and improve the photoelectric performance. The hot electrons from Au nanoparticles are injected into the $CdMoO_4$–ZnO composite film, leading to the increased photocurrent. When the light is off, the Schottky barriers formed between Au nanoparticles and $CdMoO_4$–ZnO composite film block the carrier transportation and accelerate the decay process of current. The study on Au-nanoparticle-modified $CdMoO_4$–ZnO composite film provides a facile method to construct ZnO film based PD with novel structure and high photoelectric performance.*

1. Introduction

UV radiation accounts for less than 10% of the total solar radiation, but it has huge influences on the survival and evolution of livings on the earth.[1] Moderate UV light is advantageous for human health, while excessive exposure to UV radiation can cause serious skin diseases. To detect and measure the UV radiation, semiconductor-based UV photodetector (PD) transforming UV radiation signals to electronic signals via photoelectric effect was subsequently invented and developed. Modern UV PDs have extended their potential applications in space communications, environmental monitoring, flame detection, and so on.[2] High sensitivity, high signal-to-noise ratio, high spectral selectivity, high speed, and high stability are required for high performance UV PDs.[3,4] Selecting appropriate active materials is of great importance for fabricating PDs with high performance.[5–9]

ZnO is a well-known n-type semiconductor and is widely applied in the photovoltaic, optoelectronic, and piezoelectric devices.[10–13] Owing to its wide bandgap, high exciton binding energy (60 meV), and high photoconductive characteristic, ZnO nanostructures are frequently used to construct UV PDs.[14–18] Gedamu et al. demonstrated burner flame transport synthesis (B-FTS) and crucible flame transport synthesis (C-FTS) for fabrication of the ZnO nano-microstructure-based UV photodetectors.[19] Fastest response/recovery time constant (≈32 ms) under 365 nm UV light irradiation of B-FTS-made photodetectors (on/off ratio ≈4.5×10^3 at 2.4 V) was reported. However, complicate

W. X. Ouyang, Dr. F. Teng, Prof. X. S. Fang
Department of Materials Science
Fudan University
Shanghai 200433, P. R. China
E-mail: xshfang@fudan.edu.cn
Dr. M. M. Jiang
State Key Laboratory of Luminescence and Applications
Changchun Institute of Optics
Fine Mechanics and Physics
Chinese Academy of Sciences
Changchun 130033, P. R. China

The ORCID identification number(s) for the author(s) of this article can be found under https://doi.org/10.1002/smll.201702177.

DOI: 10.1002/smll.201702177

© 2017 Wiley-VCH Verlag GmbH & Co. KGaA, Weinheim

experimental setup for C-FTS approach, a high operating temperature of 950 °C, and prepatterned chips prepared by photolithography are required to fabricate the fast UV sensors. These will surely raise the costs, make the assembly process complex, and weaken the stability of the configuration, which limit the practical application of the photodetectors. It is necessary to develop other ZnO nanostructures for practical photodetectors by easy preparation and facile assembly processes. ZnO nanoparticle films with high specific area and physical flexibilities are easy and cheap to prepare and process with low costs, and the photoconductivity of ZnO film PDs changes notably upon on–off state switching, demonstrating their potential in practical applications.[20,21] Nevertheless, ZnO film PD suffers from either low photoresponse or slow response speed, which severely limits its practical applications.[22] It is believed that the depletion layers formed by the adsorption of oxygen molecules on the surface of nanoparticles have great influences on the conductivity and response time of the ZnO film PD.[23] Many attempts to adjust the depletion layers and the behavior of the photogenerated charge carriers have been made to improve the photoresponsivity and to accelerate the response speed of the ZnO film PD.[24]

In particular, forming heterojunctions between ZnO and other materials (ZnS,[25] poly(vinyl alcohol) (PVA),[26] poly(arcylonitrile) (PAN),[27,28] and poly(vinyl carbazole) (PVK))[29] has significant effects on improving the photoelectric performance of ZnO film based PDs.[30,31] Chaaya et al. prepared a 3D polyacrylonitrile/ZnO material with a large surface area based on the combination of electrospinning and atomic layer deposition (ALD).[28] The UV photoresponse current was enhanced by a factor of 250 compared to a flat electrode.

$CdMoO_4$ is a kind of direct-gap semiconductors with a wide bandgap of ≈3.25 eV.[32,33] It has potential in a broad range of applications such as photoluminescence, scintillator materials, humidity sensors, and catalysis.[34–36] The unique combination of physical and chemical properties of $CdMoO_4$ in terms of molecular and electronic versatility, reactivity, and stability suggests that $CdMoO_4$ may have potential applications in UV PDs. To date, however, studies on the photoelectric property of $CdMoO_4$ have rarely been reported. Considering that the potential values of the conduction band and valence band of $CdMoO_4$ are more negative than those of ZnO, a type-II heterojunction can be formed between $CdMoO_4$ and ZnO.[37] It is deduced that $CdMoO_4$ may be used to improve the photoelectric performance of ZnO.

It is reported that metal nanostructures can create and inject hot electrons into coupled semiconductors, which have potential applications in solar fuel cells, photodetectors, photocatalysts, solid state lasers, etc.[38–43] Recently, the novel properties of Au nanostructures have been explored for UV PDs with enhanced performance.[44] The combination of metallic nanostructures and ZnO nanoparticles can improve the photoelectric performance of ZnO film PDs.[45] Viter et al. prepared Si/ZnO thin films modified with ultrathin gold layers of different thicknesses by the combination of ALD and physical vapor deposition (sputtering). The influence of localized plasmons on the optical properties of Au/ZnO nanostructures was demonstrated.[46] Jin reported the enhancement of UV photodetection using Au–ZnO nanocomposites prepared by a photoreduction process.[47] The enhanced UV photoresponse is attributed to the interband absorption or hole trapping ability of Au nanoparticles (NPs) within the nanocomposite. It is reported that the formation of junctions between metal nanostructures and ZnO nanoparticles can be used to adjust the depletion layer on the surface of ZnO nanoparticles, leading to decreased decay time. Jin et al. fabricated a UV PD with colloidal ZnO nanoparticles and gold electrodes. The Schottky barrier formed between ZnO nanoparticles and gold electrodes significantly modified the depletion layers and led to the decrease of the rise and decay times.[23]

Herein, novel $CdMoO_4$–ZnO composite film (CMO–ZnO) is easily prepared by dispersing $CdMoO_4$ microplates on the ZnO film to construct it into PD device. The photoelectric performances of as-constructed $CdMoO_4$–ZnO composite film PDs with different loading amounts of $CdMoO_4$ microplates are tested under illumination with 350 nm UV light, which reveals that a ≈18-fold higher responsivity and half reduced decay time can be accomplished under an optimized condition. Moreover, Au NPs are deposited on the CMO–ZnO composite film with different deposition intervals by ion sputtering to construct Au–CMO–ZnO composite film PD. The photoresponse of the Au–CMO–ZnO PD with optimized deposition time is further enhanced under illumination with 350 nm UV light at a bias of 5 V and the decay time decreases as well. The Au–CMO–ZnO composite film PD provides a facile method to construct ZnO film based PD with high performance and novel structure.

2. Results and Discussion

Scheme 1 displays the preparation process of ZnO film, CMO–ZnO composite film, and Au–CMO–ZnO composite film. ZnO film on glass was prepared by spin-coating method and annealing process. Then, the dispersion of $CdMoO_4$ was spin-coated on the ZnO film and then annealed to form CMO–ZnO composite film. Finally, Au–CMO–ZnO composite film was prepared by ion-sputtering of Au NPs on the composite film.

The X-ray diffraction (XRD) patterns of ZnO film, $CdMoO_4$ sample, and CMO–ZnO composite film are presented in **Figure 1**. The diffraction peaks of the ZnO film match well with the hexagonal phase ZnO (JCPDS 65-3411). The broadened diffraction peaks with relative weak intensity indicate that the ZnO film might be very thin and compose of nanoparticles. The sharp diffraction peaks of the $CdMoO_4$ sample with high intensity are indexed to the tetragonal phase $CdMoO_4$ (JCPDS 07-0209), which implies that the $CdMoO_4$ sample prepared by hydrothermal method is of high purity and crystallinity. For the CMO–ZnO composite film, the diffraction peaks emerging at 29.2°, 31.9°, and 34.8° correspond to the tetragonal phase $CdMoO_4$, while the diffraction peak at 34.4° is from the hexagonal phase ZnO. It is worth noticing that the diffraction peak with the highest intensity changed from (112) to (004) after the deposition of

 © 2017 Wiley-VCH Verlag GmbH & Co. KGaA, Weinheim

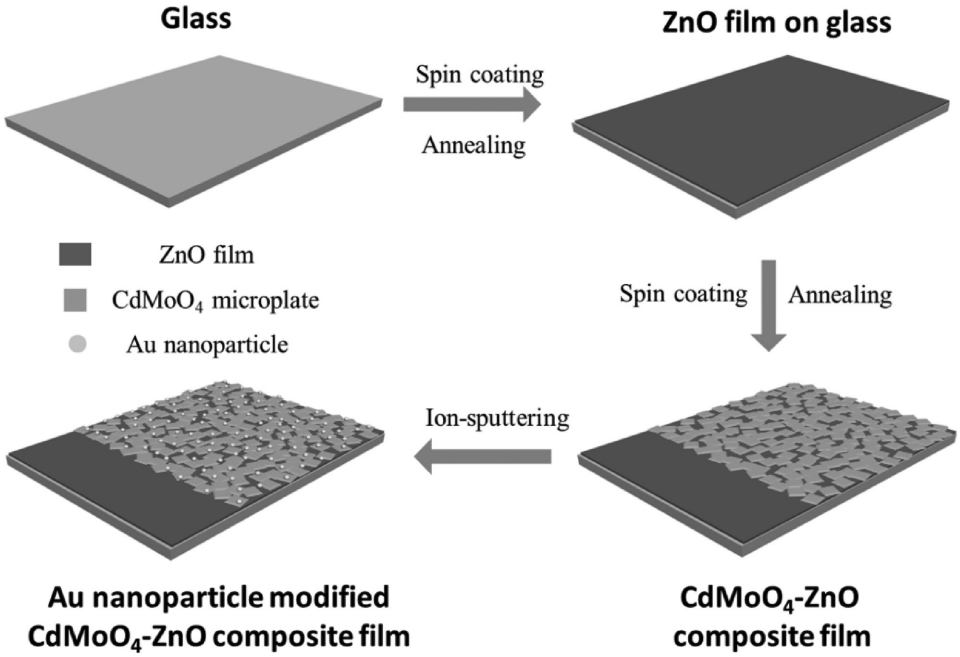

Scheme 1. Preparation process of ZnO film, CMO–ZnO composite film, and Au–CMO–ZnO composite film.

$CdMoO_4$ on ZnO film, suggesting that the orientation of the $CdMoO_4$ microplates has changed after being deposited on the ZnO film.

Figure 2 displays the scanning electron microscopy (SEM) images of the four samples. From Figure 2a,d, it is observed that the ZnO film is composed of densely packed nanoparticles with diameters of 20–50 nm, and is evenly coated on the substrate with thickness of nearly 100 nm. The atomic-force microscopy (AFM) images of the ZnO film are displayed in Figure S1 (Supporting Information), the ZnO film is even and of relatively smooth surface. As shown in Figure 2b, the $CdMoO_4$ sample is in the form of regular microplates with lateral size of 2–3 μm and thickness of 500–800 nm. These microplates present smooth, even, and flat top surfaces, which correspond well with the AFM results in Figure S2 (Supporting Information). In Figure 2c,e, it is clearly shown that the $CdMoO_4$ microplates are well dispersed and oriented on the ZnO film. The high speed spin-coating processes are essential to disperse the $CdMoO_4$ microplates evenly on the ZnO film. Due to the robust surface of the ZnO film and the high surface ratio of the $CdMoO_4$ microplates, the $CdMoO_4$ microplates tend to lay down and form contact with the ZnO film via their domain surfaces ((004) facets). Due to the large surface area of the $CdMoO_4$ microplates, the large contact area between the ZnO and $CdMoO_4$ phases facilitate their mutual interactions and will have a great influence on their electrical properties. It is observed in Figure 2f,d that, several nanoparticles with diameters of about tens of nanometers are dispersed evenly on the surface of the $CdMoO_4$ microplates after the ion sputtering of Au on the CMO–ZnO composite film. As depicted in the SEM images of samples (in Figure S3 in the Supporting Information) with different sputtering times, the amount and diameter of the nanoparticles increase with the increase of deposition times.

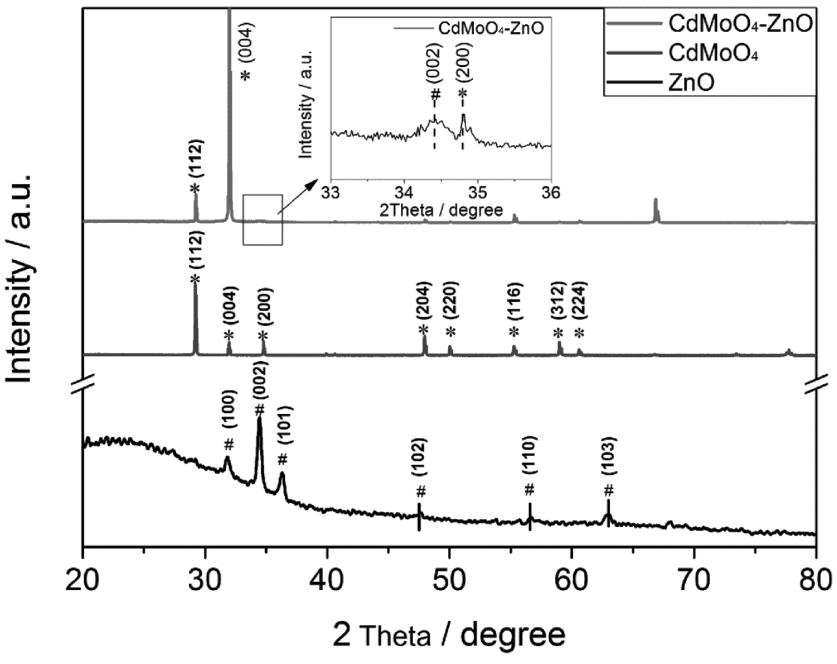

Figure 1. XRD patterns of ZnO film, $CdMoO_4$ sample, and CMO–ZnO composite film. Peaks from ZnO film are indicated with #, peaks from $CdMoO_4$ sample are marked with *.

The elemental composition and chemical state of the samples are examined by X-ray photoelectron spectroscopy (XPS). The XPS spectrum of the $CdMoO_4$ sample

 © 2017 Wiley-VCH Verlag GmbH & Co. KGaA, Weinheim

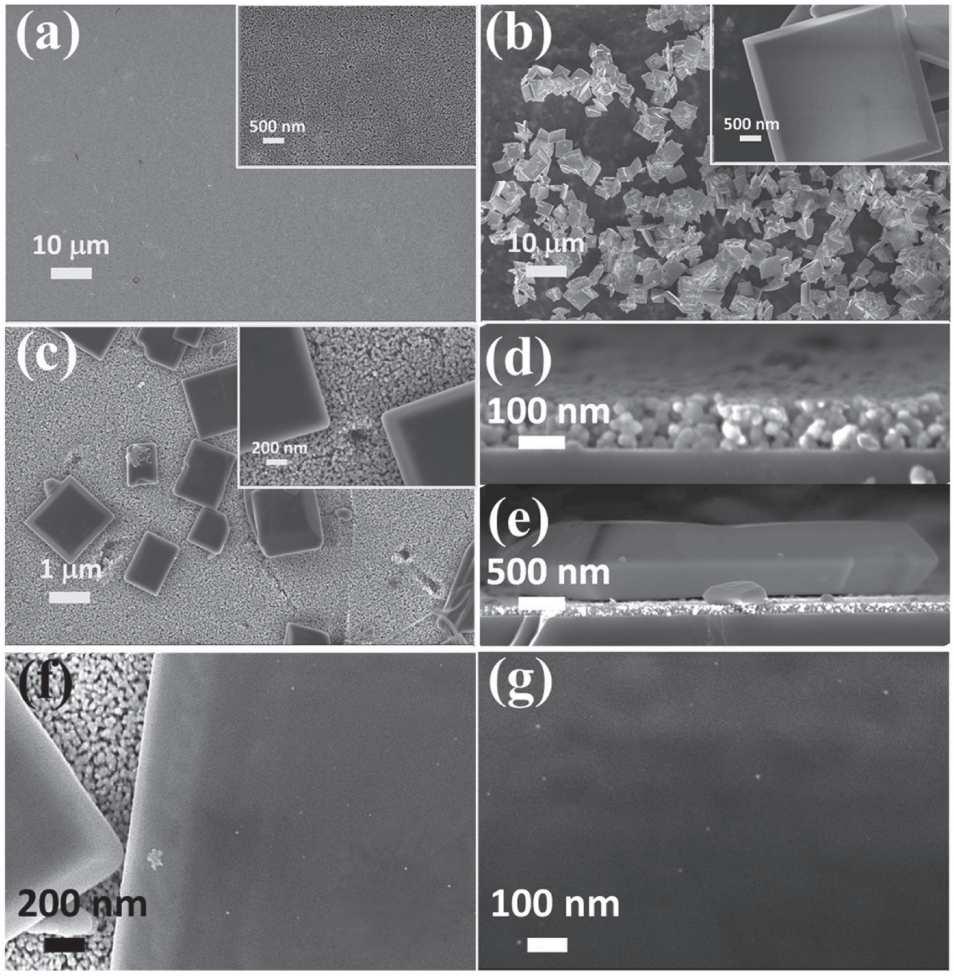

Figure 2. SEM images of a) ZnO film, b) $CdMoO_4$ sample, c) CMO–ZnO composite film, the cross-section of d) ZnO film, e) CMO–ZnO composite film, f,g) the Au-15-CMO-0.8-ZnO composite film. The inset pictures are taken with higher magnifications.

in Figure S4a (Supporting Information) confirmed the existence of the elements Cd, Mo, and O with their corresponding valence values of +2, +6, and –2. According to the XPS spectra of the Au-15-CMO-0.8-ZnO sample in Figure S4b (Supporting Information), the peaks emerging at binding energy of 84.0 eV belong to Au 4f7, which confirmed that the deposited nanoparticles are Au NPs.[48] It is obvious in Figure S4c,d (Supporting Information) that with the increase of sputtering time from 15 to 45 s, the intensity of binding energy peak of the Au 4f7 increases correspondingly, depicting the increased amount of Au NPs.

Figure 3a demonstrates the configuration of a CMO–ZnO heterojunction photodetector. The current–voltage (*I–V*) characteristics of the ZnO PD both in dark and under 350 nm UV light illumination are shown in Figure 3b. The dark current and photocurrent of the ZnO PD increase linearly with the increase of the applied bias, which illustrates that the ZnO PD is of metal–semiconductor–metal (MSM) structure. The ZnO PD yields relatively low dark current (0.48 nA at 10 V bias) and low photocurrent (11.0 nA at 10 V bias) under 350 nm UV light illumination. Figure 3c,d presents the *I–V* curves of the CMO-1.6-ZnO PD in dark and under 350 nm UV light illumination, respectively. The dark current under the forward bias of 10 V is 1.1 nA and under the reverse bias of –10 V is –0.64 nA. The photocurrent under the forward bias of 10 V is 72.4 nA and under the reverse bias of –10 V is 25.0 nA. The nonlinear relationship reveals a rectifying characteristic and demonstrates that a heterojunction is formed between ZnO film and $CdMoO_4$ microplates. The incorporation of $CdMoO_4$ microplates increases the photocurrent of CMO-1.6-ZnO PD significantly, and it is deduced that the heterojunction plays an important role in improving the photoelectric performance of the CMO–ZnO PDs.

Further investigations were conducted to examine the influences of the loading amounts of $CdMoO_4$ microplates on the photoelectric properties of CMO–ZnO PDs. **Figure 4**a compares the *I–V* characteristics of CMO–ZnO PDs and ZnO PD under dark and 350 nm UV light illumination. The ZnO film PD yields dark current of 0.1 nA and photocurrent of 10.4 nA at 5 V. With the increase of loading amount of $CdMoO_4$ sample, the photocurrents obtained at 5 V increase from 42.3 nA for CMO-0.2-ZnO PD to 73.8 nA for CMO-0.4-ZnO PD. The photocurrent of CMO-0.8-ZnO PD reaches 155.4 nA at 5 V, which is ten-fold of that of the ZnO PD, while its dark current in the whole voltage range is lower than that of ZnO PD. Continuing increasing of $CdMoO_4$ loading amount, the photocurrents then decrease to 26.9 nA for CMO-1.6-ZnO PD and 0.6 nA for CMO-2.4-ZnO PD at 5 V,

© 2017 Wiley-VCH Verlag GmbH & Co. KGaA, Weinheim

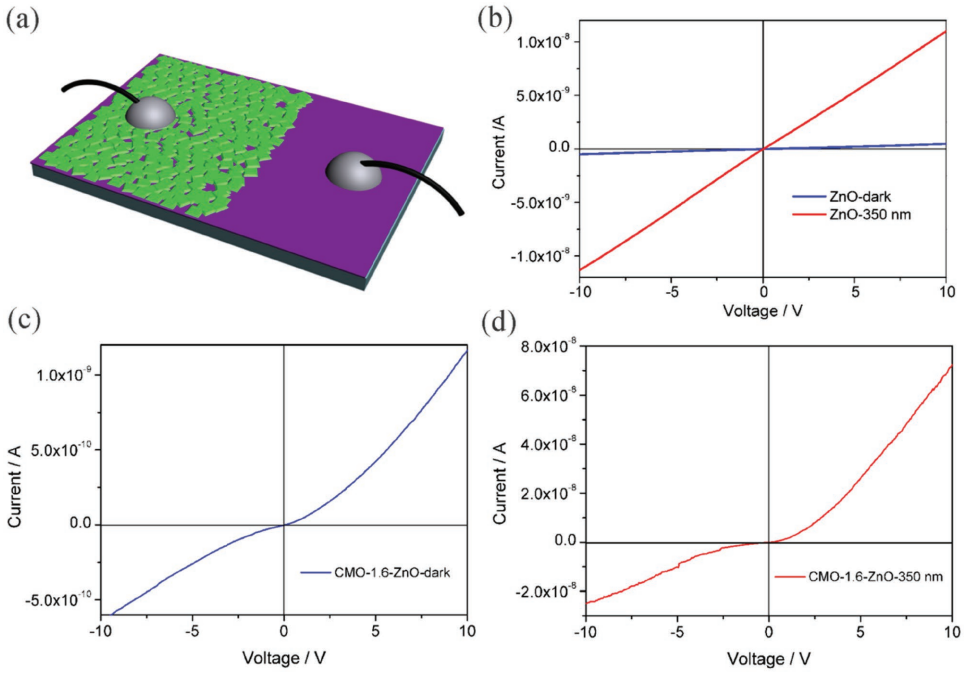

Figure 3. a) Schematic diagram of CMO–ZnO photodetector. b) *I–V* characteristics of the ZnO photodetector under dark and illumination with 350 nm UV light. *I–V* characteristics of the CMO-1.6-ZnO photodetector c) under dark and d) under illumination with 350 nm UV light.

while their dark currents become higher than that of ZnO PD. Figure 4b shows the time-dependent current curves of different PDs with on/off switching upon 350 nm light illumination under a bias of 5 V. For all the PDs, when the light is turned on, the currents immediately increase and then reach steady states. The photocurrent of ZnO PD increases gradually to 13.9 nA in 60 s. Due to the slow adsorption process of absorbed O_2 molecules on the surface of ZnO nanoparticles, the current of ZnO PD cannot recover to the original dark current in the fixed intervals upon on/off switching. Its

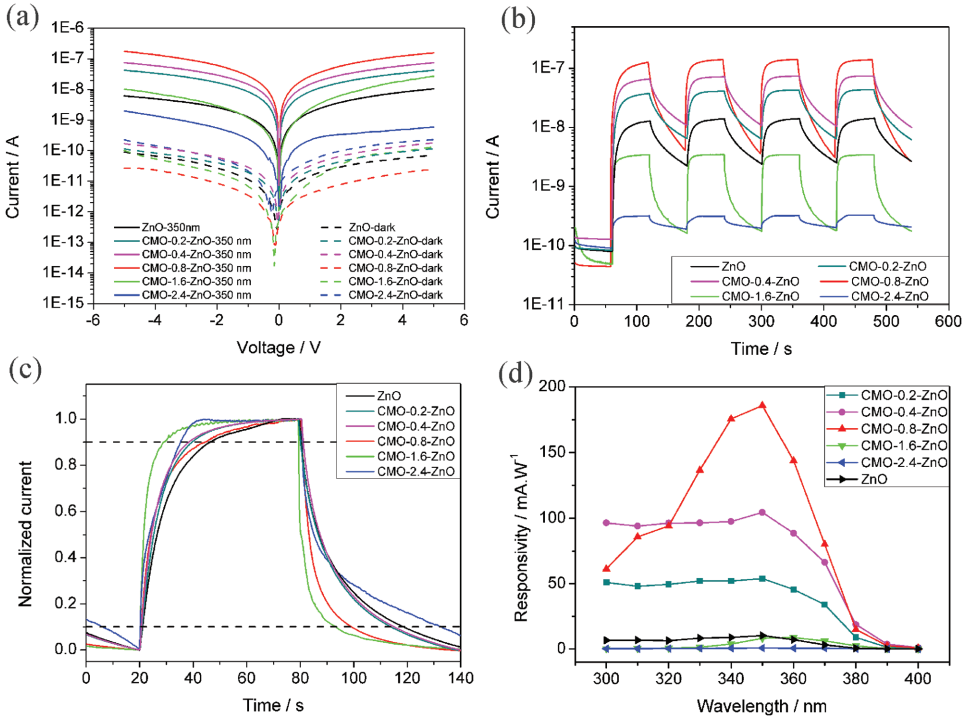

Figure 4. Comparison of photoelectric performance between CMO–ZnO photodetectors and ZnO photodetector: a) *I–V* characteristics under dark and 350 nm UV light illumination; b) *I–t* characteristics with on/off switching upon 350 nm light illumination under 5 V bias; c) the normalized *I–t* curves; d) spectral response at 5 V bias.

© 2017 Wiley-VCH Verlag GmbH & Co. KGaA, Weinheim

current decreases to 2.2 nA, leading to a low on–off ratio of 6.2. Compared with the ZnO PD, the photocurrent of $CdMoO_4$–ZnO PD loaded with 0.2 mg of $CdMoO_4$ sample increases to 40.92 nA and the on–off ratio nearly keeps the same. With the adding amount of $CdMoO_4$ sample increasing to 0.4 and 0.8 mg, the photocurrent continues to rise to 71.68 nA and then peaks at 139.4 nA, with the on–off ratio increases from 6.6 to 34.1, respectively. The further increase of adding amount to 1.6 and 2.4 mg causes the decrease of photocurrent to 3.5 and 0.3 nA, which is lower than that of the ZnO film PD. Meanwhile, the on–off ratio decreases from 21.1 to 1.7. It can be clearly seen that the currents of all these devices can be reproduced when the light source is switched on/off repeatedly. The stability of the CMO-0.8-ZnO photodetector was tested (in Figure S5a in the Supporting Information) and displayed similar photodetecting performance after many cycles, which demonstrates that the PDs have good stability. To investigate the influence of the loading amount of $CdMoO_4$ on the response time of the PDs, the *I*–*t* curves of the PDs are normalized and displayed in Figure 4c. Moreover, the characteristic parameters of PDs are calculated and summarized in **Table 1**. The calculated rise time decreases from 19.59 to 18.43 s and then to 16.63 s with the $CdMoO_4$ amount increasing from 0.2 to 0.4 mg and then to 0.8 mg, while the decay time decreases from 34.52 to 33.1 s and then to 18.96 s. The CMO-1.6-ZnO PD has the shortest rise and decay time of 10.4 and 15.1 s, while the rise and decay times of the CMO-2.4-ZnO PD increase to 15.4 and 53.7 s. Figure 4d presents the spectral response of the PDs at 5 V bias from 300 to 400 nm. The responsivities of CMO-0.2-ZnO, CMO-0.4-ZnO, and CMO-0.8-ZnO PDs increase stepwise and are significantly higher in the whole wavelength range compared with those of ZnO PD. The CMO-0.8-ZnO PD shows the highest responsivity of 185.9 mA W^{-1} under 350 nm UV light illumination at a bias of 5 V, which is 18-fold higher than that of ZnO PD. Also, the spectral responses of the CMO-0.8-ZnO PD and ZnO PD between 300 and 400 nm at 1, 3, and 5 V bias are shown in Figure S6 (Supporting Information). As the bias increases, the spectral responses of CMO-0.8-ZnO PD increase stepwise and are much higher than those of the ZnO PD under the same conditions, and the highest responsivities of those PDs are all achieved at 350 nm. To achieve a balance between the feasible detection of the current (higher applied voltage required) and the ease operating of the photodetector (lower applied voltage preferred), an applied bias voltage of 5 V is used in the later part of photoelectric measurement. The further increase of the $CdMoO_4$ amount greatly weakens the responsivities of CMO-1.6-ZnO and CMO-2.4-ZnO PDs. Thus, CMO-0.8-ZnO PD exhibits the best photoelectric performance among all five different CMO–ZnO PDs. It is concluded that the photoelectric properties of ZnO film PD can be greatly improved by loading optimized amount of $CdMoO_4$ microplates.

To further improve the photoelectric properties, Au NPs were deposited on the composite films with different deposition intervals by ion sputtering. The photoelectric performance of the Au NP modified CMO-0.8-ZnO PDs was investigated. **Figure 5**a compares the *I*–*V* characteristics of the Au-CMO-0.8-ZnO PDs and CMO-0.8-ZnO PD under dark and 350 nm UV light illumination. After the deposition of Au NPs, the photocurrents obtained at 5 V increase from 155.4 nA for CMO-0.8-ZnO PD to 286.4 nA for Au-15-CMO-0.8-ZnO PD. The further increase of deposition intervals to 30, 45, and 60 s leads to the decrease of the photocurrents obtained at a bias of 5 V to 119.9, 72.0, and 26.1 nA, respectively. Meanwhile, the dark currents of Au–CMO–ZnO PDs have decrease by one to two magnitudes compared with those of CMO-0.8-ZnO PD, which may result from the Schottky barriers formed between Au NPs and the CMO–ZnO composite film. Figure 5b shows the time-dependent current curves of the different PDs with on/off switching upon 350 nm light illumination under 5 V bias. The photocurrent increases from 139.4 to 289.1 nA after the deposition of Au NPs on CMO–ZnO composite film and the on–off ratio increases by about ten-fold to 377.2. With the deposition time of Au NPs increasing to 30, 45, and 60 s, the photocurrent begins to decrease to 131.4, 55.3, and 16.5 nA, while the on–off ratios rise up to 2182.4, 25816.0, and then drop to 1149.0, respectively. The deposition intervals of Au NPs also have a great impact on the response time of Au NP modified composite film PDs. In Figure S5 (Supporting Information), the stability of the Au-15-CMO-0.8-ZnO PD was tested and it displayed similar photodetecting performance, the morphology of the Au–CMO–ZnO composite film remains nearly the same after the photoelectric tests. These results demonstrate the good stabilities of the PDs. To further compare the response times of the PDs, the time-dependent current curves are normalized in Figure 5c and the characteristic parameters of PDs are summarized in **Table 2**. It is seen that the decay time decreases from 18.96 s (CMO–ZnO PD) to 9.2 (Au-15 s), 8.9 (Au-30 s), 1.8 (Au-45 s), and 6.2 s (Au-60 s). Figure 5d presents the spectral response of the five PDs at 5 V bias from 300 to 400 nm. Compared with the CMO-0.8-ZnO PD, the responsivity of Au-15-CMO-0.8-ZnO PD increases

Table 1. Comparison of the characteristic parameters of ZnO photodetector and different CMO–ZnO photodetectors at a bias of 5 V.

Sample	Photocurrent [nA]	Rise time [s]	Decay time [s]	On–off ratio	Responsivity (350 nm) [mA W^{-1}]
ZnO	13.9	30.06	40.2	6.2	10.4
CMO-0.2-ZnO	40.92	19.59	34.52	6.4	53.9
CMO-0.4-ZnO	71.68	18.43	33.1	6.6	104.5
CMO-0.8-ZnO	139.4	16.63	18.96	34.1	185.9
CMO-1.6-ZnO	3.5	10.4	15.1	21.1	8.3
CMO-2.4-ZnO	0.3	15.4	53.7	1.7	0.8

© 2017 Wiley-VCH Verlag GmbH & Co. KGaA, Weinheim

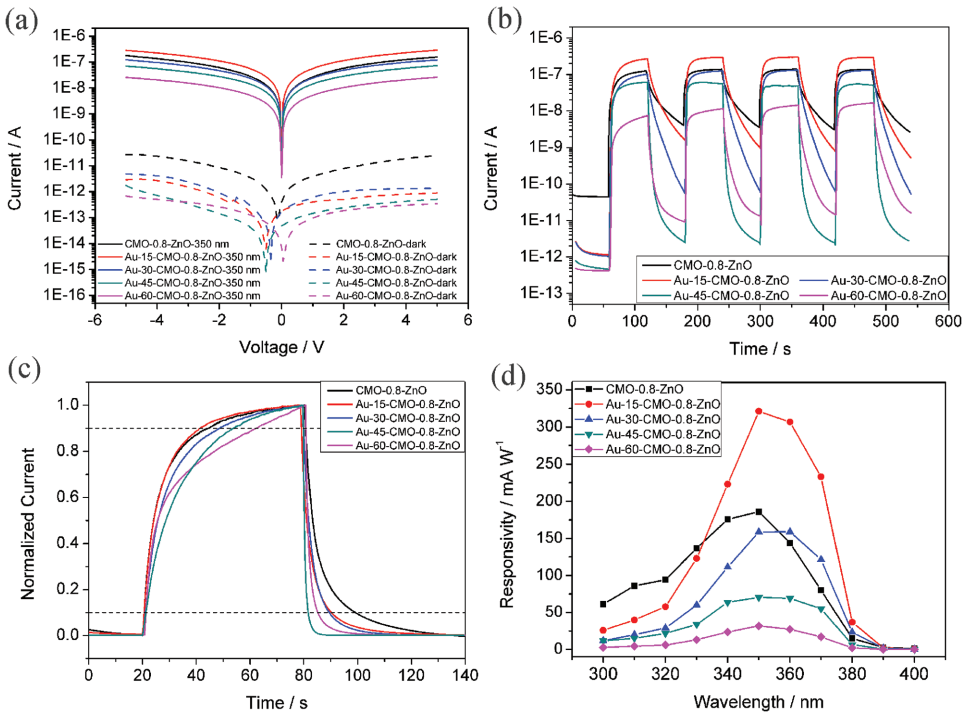

Figure 5. Comparison of photoelectric performance between Au–CMO–ZnO photodetectors and CMO-0.8-ZnO photodetector: a) *I–V* characteristics under dark and 350 nm UV light illumination; b) *I–t* characteristics with on/off switching upon 350 nm light illumination under 5 V bias; c) the normalized *I–t* curves; d) spectral response at 5 V bias.

greatly from 340 to 400 nm, and the highest responsivity of 321.1 mA W^{-1} is achieved under 350 nm UV light illumination at a bias of 5 V. With the increase of deposition intervals, the spectral responses of the Au–CMO–ZnO PDs decrease gradually. It is believed that deposition of the proper amount of Au NPs has improved the photoelectric performance of the CMO–ZnO PDs, while the excess amount of Au NPs will weaken the photoresponse greatly.

To examine the influence of different metal nanoparticles on the photoelectric properties of CMO–ZnO composite film PDs, Al and Ag nanoparticles were sputtered on the CMO–ZnO composite film under the same sputtering conditions and the deposition interval was fixed to 15 s. The XPS spectra shown in Figure S7 (Supporting Information) demonstrate the existences of element Ag in the composite films, while the binding energy peak of Al 2p is too weak to be detected in the XPS characterization.[49,50] The comparisons of photoelectric performance between different metal nanoparticle modified CMO–ZnO composite film PDs and CMO-0.8-ZnO PD are presented in Figure S8 (Supporting Information). It is demonstrated that both the photocurrents and decay time of CMO–ZnO composite film PDs decrease after Al and Ag nanoparticle modification, while the photoresponses of Ag and Al nanoparticle modified CMO–ZnO PDs in the wavelength range from 300 to 400 nm are much smaller than those of the Au–CMO–ZnO PD. Under the same sputtering conditions, Au nanoparticles are more suitable for improving the photoelectric performance of CMO–ZnO composite film PDs than Al and Ag nanoparticles.

The role of $CdMoO_4$ microplates and Au NPs in improving the photoelectric properties of Au–$CdMoO_4$–ZnO PDs has been investigated in detail as follows.

To examine the function of $CdMoO_4$ in the composite film PDs, a $CdMoO_4$ film PD was constructed (Figure S9a, Supporting Information) and its photoelectric performance was tested. Figure S10b (Supporting Information) shows the UV–visible absorption and reflection spectra of the 0.8 mg $CdMoO_4$ sample, and it is demonstrated that the absorption of $CdMoO_4$ sample is mainly located in the UV zone. As inferred from the inset, the bandgap of the $CdMoO_4$ sample is calculated to be 3.25 eV, which corresponds well with previous reports.[51,52] Figure S9b (Supporting Information) presents

Table 2. Comparison of the characteristic parameters of CMO–ZnO photodetector and different Au–CMO–ZnO photodetectors at a bias of 5 V.

Sample	Photocurrent [nA]	Rise time [s]	Decay time [s]	On–off ratio	Responsivity (350 nm) [mA W^{-1}]
CMO-0.8-ZnO	139.4	16.63	18.96	34.1	185.9
Au-15-CMO-0.8-ZnO	289.1	16	9.2	377.2	321.1
Au-30-CMO-0.8-ZnO	131.4	15.8	8.9	2182.4	158.6
Au-45-CMO-0.8-ZnO	55.3	32.6	1.8	25 816.0	70.4
Au-60-CMO-0.8-ZnO	16.5	29.3	6.2	1149.0	31.8

© 2017 Wiley-VCH Verlag GmbH & Co. KGaA, Weinheim

the *I–V* characteristics of the $CdMoO_4$ film PDs in dark and under 350 nm UV light illumination. The photocurrents of the PDs are almost coincident with the dark currents. Figure S9c (Supporting Information) shows the time-dependent currents of different PDs under 5 V bias. Although the photocurrents immediately increase and reach steady states once the illumination is turned on, the UV response of the 0.8 mg $CdMoO_4$ PD can be neglected compared with that of ZnO film PD. It is supposed that the poor transportation of carriers between nearby microplates accounts for the poor photoelectric performance of $CdMoO_4$ film PDs.

Compared with the ZnO film and $CdMoO_4$ film PDs, the CMO-0.8-ZnO PD shows greatly improved photoelectric performance. As shown in Figure S10a,b (Supporting Information), due to the wide bandgaps of ZnO and $CdMoO_4$, ZnO film and $CdMoO_4$ microplates are photoexcited under the illumination of UV light. The bandgap of ZnO and $CdMoO_4$ are determined to be ≈3.2 and ≈3.25 eV according to their UV–vis spectra (insets in Figure S10a,b in the Supporting Information). It is deduced from the valence band XPS spectra (Figure S10c,d, Supporting Information) that the valence band of ZnO is of 1.6 eV lower relative to its Femi energy band and the valence band of $CdMoO_4$ is of 1.26 eV lower relative to its Femi energy band. The Femi energy bands of ZnO and $CdMoO_4$ are aligned at the same position after the formation of heterojunction. Then, it is deduced that the conduction band of ZnO is of 1.6 eV higher than the Femi energy band, and the conduction band of $CdMoO_4$ is of 2 eV higher than the Femi energy band. It is concluded that the conduction band of $CdMoO_4$ is of ≈0.4 eV higher than that of ZnO, thus a type-II heterojunction forms between ZnO and $CdMoO_4$ and the aligned schematic band diagram for $CdMoO_4$–ZnO heterojunction is presented in Figure S10e (Supporting Information). The photoelectrons in the conduction band of $CdMoO_4$ flow into that of ZnO, which increases the concentration of electrons in ZnO film and leads to the increase of photocurrents, the built-in electron field at the interface blocks the direct transport path of electrons between the electrodes, which promote the decay of photocurrent as soon as the UV illumination is off. To get more insight into the photodetector mechanism, electric potential field distribution on account of ZnO film based MSM structure, and CMO decorated ZnO film based heterojunction are numerically simulated in **Figure 6** (or Figure S11 in Supporting Information) based on the semiconducting model. For the ZnO film PD, the potential drop distributes evenly in the ZnO film located between the electrodes, which is not facilitative for the separation of charge carriers and easy for the recombination and depletion of electron and hole in defects. Hence, ZnO MSM PD shows poor photoelectric performance. For the CMO–ZnO PDs, the potential drop mainly occurs at the interfaces between the $CdMoO_4$ microplates and the ZnO film. The inner electrical field formed between ZnO and $CdMoO_4$ facilitates the separation and transportation of charge carriers. The recombination and depletion of electrons and holes on their pathway to electrodes are reduced, leading to improved photoelectric properties of $CdMoO_4$–ZnO heterojunction PD. These results coincide well with the experimental results and demonstrate that the

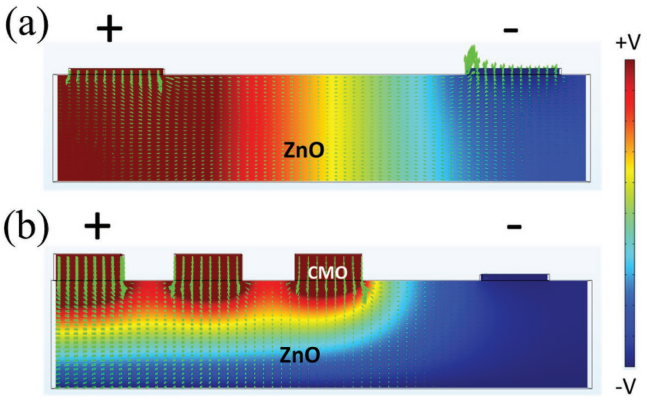

Figure 6. Simulated electric potential distribution and electron trackings of a) the ZnO PD with MSM structure and b) the CMO–ZnO PD with heterojunction structure.

formation of heterojunction and the change of PD structures from MSM to heterojunction type improve the photoelectric performance of the CMO–ZnO PD.

Figure S12a (Supporting Information) presents the UV–visible absorption and reflection spectra of different CMO–ZnO composite samples, and it is illustrated that excess loading of $CdMoO_4$ microplates would significantly shelter the ZnO film underneath and block the light absorption of the composite film, which leads to the decrease of photocurrents. To eliminate the shading effect of $CdMoO_4$ microplates on the ZnO film, the CMO-1.6-ZnO PD is irradiated from the backside. As shown in Figure S12b (Supporting Information), its photoresponsivities increase greatly and become even higher than those of ZnO PD. It demonstrates that the shading effect of $CdMoO_4$ is the main cause for the decrease of photoresponsivities of the composite film PDs with the excess loading of $CdMoO_4$ microplates.

It is reported that the junctions between metal nanostructures and ZnO nanoparticles can be used to adjust the depletion layer on the surface of ZnO nanoparticles to modify the ZnO film PD.[47] Figure S13 (Supporting Information) compares the photoelectric performance between Au–ZnO PDs and ZnO PD. For pure ZnO film, the adsorption of oxygen molecules on the surface of ZnO nanoparticles causes the formation of depletion layers with low conductivity, which has great influences on the conductivity and response time of the ZnO PD. The slow adsorption and desorption process of oxygen molecules leads to the long decay and rise times of ZnO PD.[24] The deposition of Au NPs leads to the formation of Schottky barriers between the ZnO film and Au NPs, which gradually decreases the photocurrents with the increasing of deposition time. When the UV light is off, the carrier transportation is blocked by the Schottky barriers formed between Au NPs and ZnO film, which promotes the decay of the current. As the deposition time increases, the increased amount and size of Au NPs strengthens the Schottky barriers and Au NPs become the recombination centers of charge carriers. These factors lead to the successive reduction of decay time, and the gradual decrease of photocurrents.

Compared with the CMO–ZnO PDs and the Au–ZnO PDs, the photoelectric performance of Au–CMO–ZnO PDs is further improved. Au NPs would form Schottky barriers

© 2017 Wiley-VCH Verlag GmbH & Co. KGaA, Weinheim

with ZnO film and $CdMoO_4$ microplates upon contacting. The formation of Schottky barriers decreases the concentration of charge carrier in the system and leads to the dramatic decrease of dark currents. Under the UV light illumination, the photocurrent of Au-15-CMO-0.8-ZnO composite film is further enhanced due to the hot electron injection effect of the Au NP,[44] which can be confirmed by the photoluminescence (PL) spectrum. Figure S14 (Supporting Information) presents the PL spectrum of ZnO film, $CdMoO_4$ film, and Au–CMO–ZnO composite film with the excitation wavelength of 314 nm. The $CdMoO_4$ film exhibits an emission peak centered at 525 nm.[51] After the deposition of Au NPs, the intensity of the emission peak of Au–CMO–ZnO composite film centered at 525 nm becomes much stronger, which demonstrates the injection of hot electrons from Au NPs to $CdMoO_4$ microplates. For Au nanostructures, the threshold for the d to s interband transition is ≈2.4 eV, the aligned schematic band diagram for Au NP modified $CdMoO_4$–ZnO heterostructure is presented in Figure S10e (Supporting Information). Upon light illumination with energy higher than 2.4 eV, hot electrons with a wide energy distribution range between 1 and 4 eV primarily generate through the intraband transitions in Au NPs.[53] Hot electrons with energies larger than the Schottky barrier at the Au–semiconductor interface will be injected to the adjacent semiconductor. For the Au–$CdMO_4$ composite, it is reported that the hot electron transfer can occur when the wavelength of the irradiated light is lower than 443 nm.[54] As displayed in **Figure 7**, under the illumination of UV light ($\lambda < 400$ nm), the hot electrons will generate in Au NPs and be injected into the conduction band of $CdMoO_4$. Then, the hot electrons together with the photoelectrons at conduction band of $CdMoO_4$ will flow into the conduction band of ZnO in cascade. The concentration of electrons in the system increases, and it leads to the enhancement of photocurrent. When the UV light is off, the Schottky barriers formed between Au NPs and the CMO–ZnO composite film will block the carrier transportation, which promotes the decay of the current.[55]

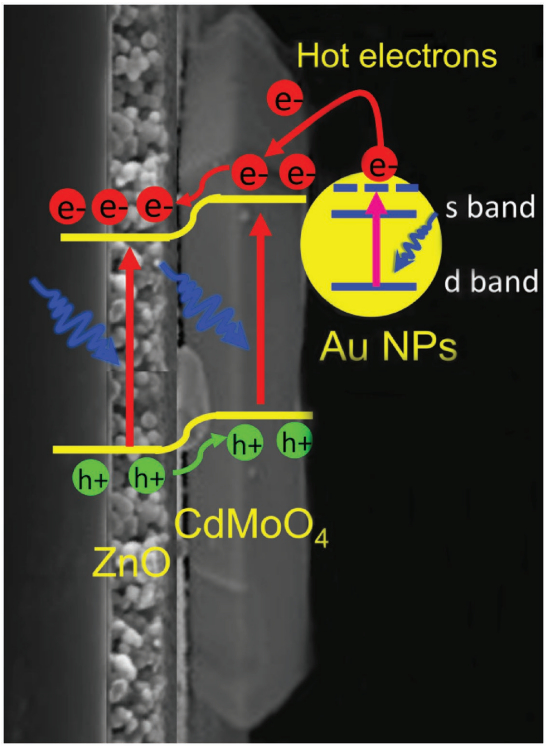

Figure 7. Proposed mechanism for the improved photoelectric performance of Au–CMO–ZnO photodetector.

As displayed in the SEM images of samples with different deposition times of Au, with the deposition time prolonging, the amount and size of the Au NPs increase, which leads to the increase of the height of Schottky barriers and the thickness of the depletion layer. It is demonstrated in Figure S14 (Supporting Information) that the hot electron injection from the Au NPs to $CdMoO_4$ is gradually weakened. Moreover, the injected hot electrons in conduction band of $CdMoO_4$ may be transferred to the electron-deficient Au NPs, returning to its ground state. These factors cause the successive decrease of decay time and photocurrent.[21]

The comparison of photoelectric performances between Au–ZnO PDs and Au–CMO–ZnO PDs also demonstrates that the $CdMoO_4$ microplates are indispensable in the photocurrent improvement of Au-15-CMO-0.8-ZnO PD. Moderate $CdMoO_4$ microplates could not only form heterojunctions with the ZnO film and inject photoelectrons into the system upon UV illumination, but also transfer the photoelectrons from the Au NPs to the ZnO film to decrease the depletion of charge carriers in the Schottky barriers.

3. Conclusion

$CdMoO_4$ microplates were synthesized via a hydrothermal process and spin-coated on the ZnO film to prepare the $CdMoO_4$–ZnO composite film. The obtained composite film was constructed as PD, and its photoelectric performance was greatly improved compared with ZnO film PD. The CMO–ZnO PD with optimized loading amount of $CdMoO_4$ microplates (CMO-0.8-ZnO) shows the highest photocurrent of 139.4 nA with a decay time of only 18.96 s and achieves a high responsivity of 185.9 mA W^{-1} under 350 nm UV light illumination. With the aid of $CdMoO_4$ microplates, the structure of the photodetector changes from MSM type to heterojunction one, which largely benefits the photoelectric performance. The heterojunction makes photoelectrons of $CdMoO_4$ microplates flowing into the ZnO film, leading to the increase of photocurrent under UV light illumination, and blocks the transportation of the electrons in the composite film after the UV light is off, causing the decrease of decay time. While, excess loading of $CdMoO_4$ microplates would significantly shelter the ZnO film underneath and block the light absorption of the composite film, which leads to the decrease of photocurrents. Moreover, the appropriate amount of Au NPs was then deposited on the CMO–ZnO composited film, which further improves photoelectric properties. Compared with the CMO–ZnO PD, the Au-15-CMO-0.8-ZnO PD achieves a higher photocurrent of 289.1 nA and a higher responsivity of 321.1 mA W^{-1}. At the same time, its decay time decreases to 9.2 s. The hot electron injection effect of Au NPs injects photoelectrons into the system and

© 2017 Wiley-VCH Verlag GmbH & Co. KGaA, Weinheim

increases the photocurrent. Meanwhile, the Schottky barriers formed between the Au NPs and CMO–ZnO composite film block the carrier transportation and accelerate the decay process of current. The study on Au–CMO–ZnO composite film PD paves the way for facile construction of ZnO film based PD with novel structure and high photoelectric performance.

4. Experimental Section

Preparation of ZnO Film on Glass: In a typical preparation process of ZnO film on glass, 1.44 g of $Zn(Ac)_2.2H_2O$ and 0.75 g of PVA-1788 (low-viscosity, M_w = 44.05) were dissolved in 10 mL of mixed solvent of H_2O and ethanol ($V_{water}/V_{ethanol}$ = 9:1). 0.2 mL of acetic acid was then added to restrain the hydrolysis of zinc salt. After stirring for 30 min, the mixture solution was spin-coated on several pieces of clean glass substrate at a speed of 3000 rpm for 20 s. The samples were then annealed in air at 400 °C for 2 h with a heating rate of 3 °C min^{-1} to form the ZnO film.

Synthesis of $CdMoO_4$ Sample: 0.192 g of $CdCl_2.2.5H_2O$ was dissolved in 30 mL of H_2O to form solution A, while 0.272 g of $(NH_4)_6Mo_7O_{24}.4H_2O$ and 0.5844 g of NaCl were dissolved in 30 mL of H_2O to form solution B. Then, solution B was added dropwise to solution A under stirring. After being stirred for 10 min, the mixed solution was placed into 100 mL Teflon-lined stainless autoclave and heated at 200 °C for 2 h. After being centrifuged, washed, and dried in vacuum, the $CdMoO_4$ sample was obtained.

Preparation of CMO–ZnO Composite Samples: Different amounts of as-obtained $CdMoO_4$ sample and 0.5 mg of poly(vinyl pyrrolidone) (PVP, M_w = 55 000) were dispersed into 10 mL of ethanol. Then, the dispersions were spin-coated on several ZnO film samples, and finally annealed in air at 400 °C for 2 h to form CMO–ZnO composite with different loadings of $CdMoO_4$. The composites with different input amounts of $CdMoO_4$ of 0.2, 0.4, 0.8, 1.6, and 2.4 mg were denoted as CMO-0.2-ZnO, CMO-0.4-ZnO, CMO-0.8-ZnO, CMO-1.6-ZnO, and CMO-2.4-ZnO, respectively.

Preparation of Au-$CdMoO_4$–ZnO Composite Samples: Au NPs were deposited on CMO–ZnO composite samples by ion sputtering method. By varying the deposition time, Au–CMO–ZnO composite samples with different amounts of Au NPs were prepared. The CMO-0.8-ZnO sample was chosen as the precursor. The samples with various deposition times of 15, 30, 45, and 60 s were denoted as Au-15-CMO-0.8-ZnO, Au-30-CMO-0.8-ZnO, Au-45-CMO-0.8-ZnO, and Au-60-CMO-0.8-ZnO, respectively.

Analysis Instruments: The crystal structures of the samples were confirmed by XRD using a Bruker D8-A25 diffractometer using Cu Kα radiation (λ = 1.5405 Å). The morphology of the as-prepared samples was examined by field-emission scanning electron microscopy (Zeiss Sigma). The AFM characterization was conducted on a Bruker Dimension Icon atomic force microscopy. The elemental composition and chemical state of the samples were measured by XPS using a Perkin Elmer PHI 5000 C ESCA system equipped with a hemispherical electron energy analyzer. UV–vis spectroscopy was conducted with a Hitachi U3900H spectrophotometer using Al_2O_3 as a reference. PL emission spectra were recorded under ambient conditions (Horiba, Fluoromax-4) with an excitation light at 314 nm induced by a He–Cd laser source.

Photoelectric Measurements: To construct photodetectors, two small pieces of silver pastes with fixed areas and distance were doctoral-bladed onto the films as electrodes. The photoelectric properties of the as-constructed PDs such as the current–voltage characteristic and the current–time transient response testing were characterized with a program-controlled semiconductor characterization system (Keithley 4200, USA). A 450 W Xe lamp equipped with a monochromator was used as the light source and the light intensity was measured with a NOVA II power meter (OPHIR Photonics). All the measurements were performed under ambient conditions.

Supporting Information

Supporting Information is available from the Wiley Online Library or from the author.

Acknowledgements

The work was supported by the National Natural Science Foundation of China (Grant Nos. 11674061 and 51471051), the Science and Technology Commission of Shanghai Municipality (15520720700), the Shanghai Shu Guang Project (12SG01), the Programs for Professor of Special Appointment (Eastern Scholar) at Shanghai Institutions of Higher Learning.

Conflict of Interest

The authors declare no conflict of interest.

[1] P. E. Glaser, *Science* **1968**, *162*, 857.
[2] H. Chen, K. Liu, L. Hu, A. A. Al-Ghamdi, X. S. Fang, *Mater. Today* **2015**, *18*, 493.
[3] L. Peng, L. Hu, X. S. Fang, *Adv. Mater.* **2013**, *25*, 5321.
[4] G. Konstantatos, E. H. Sargent, *Nat. Nanotechnol.* **2010**, *5*, 391.
[5] X. S. Fang, L. F. Hu, K. F. Huo, B. Gao, L. J. Zhao, M. Y. Liao, P. K. Chu, Y. Bando, D. Golberg, *Adv. Funct. Mater.* **2011**, *21*, 3907.
[6] R. Velazquez, A. Aldalbahi, M. Rivera, P. Feng, *AIP Adv.* **2016**, *6*, 085117.
[7] A. J. Molinamendoza, A. Moya, R. Frisenda, S. A. Svatek, P. Gant, S. Gonzalezabad, E. Antolin, N. Agraït, G. Rubiobollinger, D. P. D. Lara, *J. Mater. Chem. C* **2016**, *4*, 10707.
[8] C. Soci, A. Zhang, B. Xiang, S. A. Dayeh, D. P. R. Aplin, J. Park, X. Y. Bao, Y. H. Lo, D. Wang, *Nano Lett.* **2007**, *7*, 1003.
[9] L. Sang, M. Liao, M. Sumiya, *Sensors* **2013**, *13*, 10482.
[10] Ü. Özgür, Y. I. Alivov, C. Liu, A. Teke, M. A. Reshchikov, S. Doğan, V. Avrutin, S. J. Cho, H. Morkoç, *J. Appl. Phys.* **2005**, *98*, 041301.
[11] Y. X. Yu, W. X. Ouyang, Z. T. Liao, B. B. Du, W. D. Zhang, *ACS Appl. Mater. Interfaces* **2014**, *6*, 8467.
[12] W. X. Ouyang, Y. X. Yu, W. D. Zhang, *Phys. Chem. Chem. Phys.* **2015**, *17*, 14827.
[13] Z. L. Wang, J. Song, *Science* **2006**, *312*, 242.
[14] K. Liu, M. Sakurai, M. Aono, *Sensors* **2010**, *10*, 8604.
[15] B. Zhao, F. Wang, H. Chen, L. Zheng, L. Su, D. Zhao, X. S. Fang, *Adv. Funct. Mater.* **2017**, *27*, 1700264.
[16] H. Y. Chen, K. W. Liu, X. Chen, Z. Z. Zhang, M. M. Fan, M. M. Jiang, X. H. Xie, H. F. Zhao, D. Z. Shen, *J. Mater. Chem. C* **2014**, *2*, 9689.

 © 2017 Wiley-VCH Verlag GmbH & Co. KGaA, Weinheim

[17] K. Hu, F. Teng, L. X. Zheng, P. P. Yu, Z. M. Zhang, H. Y. Chen, X. S. Fang, *Laser Photonics Rev.* **2017**, *11*, 1600257.
[18] N. Liu, G. Fang, W. Zeng, H. Zhou, F. Cheng, Q. Zheng, L. Yuan, X. Zou, X. Zhao, *ACS Appl. Mater. Interfaces* **2010**, *2*, 1973.
[19] D. Gedamu, I. Paulowicz, S. Kaps, O. Lupan, S. Wille, G. Haidarschin, Y. K. Mishra, R. Adelung, *Adv. Mater.* **2014**, *26*, 1541.
[20] K. W. Liu, J. G. Ma, J. Y. Zhang, Y. M. Lu, D. Y. Jiang, B. H. Li, D. X. Zhao, Z. Z. Zhang, B. Yao, D. Z. Shen, *Solid-State Electron.* **2007**, *51*, 757.
[21] F. Teng, L. Zheng, K. Hu, H. Chen, Y. Li, Z. Zhang, X. S. Fang, *J. Mater. Chem. C* **2016**, *4*, 8416.
[22] D. Jiang, J. Zhang, Y. Lu, K. Liu, D. Zhao, Z. Zhang, D. Shen, X. Fan, *Solid-State Electron.* **2008**, *52*, 679.
[23] Y. Jin, J. Wang, B. Sun, J. C. Blakesley, N. C. Greenham, *Nano Lett.* **2008**, *8*, 1649.
[24] Z. Jin, Q. Zhou, Y. Chen, P. Mao, H. Li, H. Liu, J. Wang, Y. Li, *Adv. Mater.* **2016**, *28*, 3697.
[25] L. Hu, M. Chen, W. Shan, T. Zhan, M. Liao, X. S. Fang, X. Hu, L. Wu, *Adv. Mater.* **2012**, *24*, 5872.
[26] M. Wang, Y. Lian, X. Wang, *Curr. Appl. Phys.* **2009**, *9*, 189.
[27] I. Iatsunskyi, A. Vasylenko, R. Viter, M. Kempiński, G. Nowaczyk, S. Jurga, M. Bechelany, *Appl. Surf. Sci.* **2017**, *411*, 494.
[28] A. A. Chaaya, M. Bechelany, S. Balme, P. Miele, *J. Mater. Chem. A* **2014**, *2*, 20650.
[29] S. W. Lee, S. H. Cha, K. J. Choi, B. H. Kang, J. S. Lee, S. W. Kim, J. S. Kim, H. M. Jeong, S. A. Gopalan, D. H. Kwon, *Sensors* **2016**, *16*, 74.
[30] H. Chen, H. Liu, Z. Zhang, K. Hu, X. S. Fang, *Adv. Mater.* **2016**, *28*, 403.
[31] F. Teng, W. Ouyang, Y. Li, L. Zheng, X. S. Fang, *Small* **2017**, *13*, 1700156.
[32] L. Zhou, W. Wang, H. Xu, S. Sun, *Cryst. Growth Des.* **2008**, *8*, 3595.
[33] W. S. Wang, L. Zhen, W. Z. Shao, Z. L. Chen, *Mater. Lett.* **2014**, *131*, 292.
[34] W. Wang, J. Cui, P. Wang, L. Zhen, W. Shao, Z. Chen, *RSC Adv.* **2014**, *4*, 38527.
[35] W. S. Wang, L. Zhen, C. Y. Xu, W. Z. Shao, *Cryst. Growth Des.* **2009**, *9*, 1558.
[36] W. S. Wang, L. Zhen, C. Y. Xu, W. Z. Shao, Z. L. Chen, *CrystEngComm* **2013**, *15*, 8014.
[37] P. Madhusudan, J. Zhang, B. Cheng, J. Yu, *Phys. Chem. Chem. Phys.* **2015**, *17*, 15339.
[38] X. N. Xie, Y. L. Zhong, M. S. Dhoni, Y. Xie, K. P. Loh, C. H. Sow, W. Ji, A. T. S. Wee, *J. Appl. Phys.* **2010**, *107*, 053510.
[39] L. B. Luo, W. J. Xie, Y. F. Zou, Y. Q. Yu, F. X. Liang, Z. J. Huang, K. Y. Zhou, *Opt. Express* **2015**, *23*, 12979.
[40] Y. Yu, Z. Ji, S. Zu, B. Du, Y. Kang, Z. Li, Z. Zhou, K. Shi, Z. Fang, *Adv. Funct. Mater.* **2016**, *26*, 6394.
[41] W. Hou, S. B. Cronin, *Adv. Funct. Mater.* **2013**, *23*, 1612.
[42] J. Qi, X. Dang, P. T. Hammond, A. M. Belcher, *ACS Nano* **2011**, *5*, 7108.
[43] B. Balamurugan, T. Maruyama, *Appl. Phys. Lett.* **2005**, *87*, 115507.
[44] N. Gogurla, A. K. Sinha, S. Santra, S. Manna, S. K. Ray, *Sci. Rep.* **2014**, *4*, 6483.
[45] A. Rajan, G. Kaur, A. Paliwal, H. K. Yadav, V. Gupta, M. Tomar, *J. Phys. D: Appl. Phys.* **2014**, *47*, 425102.
[46] R. Viter, Z. Balevicius, A. A. Chaaya, I. Baleviciute, S. Tumenas, L. Mikoliunaite, A. Ramanavicius, Z. Gertnere, A. Zalesska, V. Vataman, V. Smyntyna, D. Erts, P. Miele, M. Bechelany, *J. Mater. Chem. C* **2015**, *3*, 6815.
[47] Z. Jin, L. Gao, Q. Zhou, J. Wang, *Sci. Rep.* **2014**, *4*, 4268.
[48] A. Y. Klyushin, T. C. Rocha, M. Havecker, A. Knop-Gericke, R. Schlogl, *Phys. Chem. Chem. Phys.* **2014**, *16*, 7881.
[49] Q. Xiang, G. Meng, Y. Zhang, J. Xu, P. Xu, Q. Pan, W. Yu, *Sens. Actuators, B* **2010**, *143*, 635.
[50] H. Piao, M. Suominen Fuller, D. Miller, N. S. McIntyre, *Appl. Surf. Sci.* **2002**, *187*, 266.
[51] G. Xing, Y. Xu, C. Zhao, Y. Wang, Y. Li, Z. Wu, T. Liu, G. Wu, *Powder Technol.* **2011**, *213*, 109.
[52] L. Zhao, L. Zhang, H. Lin, Q. Nong, M. Cui, Y. Wu, Y. He, *J. Hazard. Mater.* **2015**, *299*, 333.
[53] X. C. Ma, Y. Dai, L. Yu, B. B. Huang, *Light: Sci. Appl.* **2016**, *5*, e16017.
[54] J. Bi, Z. Zhou, M. Chen, S. Liang, Y. He, Z. Zhang, L. Wu, *Appl. Surf. Sci.* **2015**, *349*, 292.
[55] A. Pescaglini, A. Martín, D. Cammi, G. Juska, C. Ronning, E. Pelucchi, D. Iacopino, *Nano Lett.* **2014**, *14*, 6202.

Received: June 26, 2017
Published online: August 22, 2017

 © 2017 Wiley-VCH Verlag GmbH & Co. KGaA, Weinheim